doi:10.1016/j.jmb.2010.06.053 J. Mol. Biol. (2010) 402, 311–325

JMB

Available online at www.sciencedirect.com

ScienceDirect

ELSEVIER

Structural Similarity between the Prion Domain of HET-s and a Homologue Can Explain Amyloid Cross-Seeding in Spite of Limited Sequence Identity

Christian Wasmer[1], Agnes Zimmer[2], Raimon Sabaté[3], Alice Soragni[1], Sven J. Saupe[3], Christiane Ritter[2] and Beat H. Meier[1]*

[1]*Physical Chemistry, ETH Zurich, Wolfgang-Pauli-Strasse 10, CH-8093 Zurich, Switzerland*

[2]*Helmholtz Centre for Infection Research, 38124 Braunschweig, Germany*

[3]*Laboratoire de Genetique Moleculaire des Champignons, IBGC UMR CNRS 5095, Universite de Bordeaux 2, Bordeaux, France*

Received 6 April 2010; received in revised form 22 June 2010; accepted 26 June 2010
Available online 1 July 2010

Edited by S. Radford

We describe a distant homologue of the fungal HET-s prion, which is found in the fungus *Fusarium graminearum*. The domain FgHET-s(218–289), which corresponds to the prion domain in HET-s from *Podospora anserina*, forms amyloid fibrils *in vitro* and is able to efficiently cross-seed HET-s(218–289) prion formation. We structurally characterize FgHET-s(218–289), which displays 38% sequence identity with HET-s(218–289). Solid-state NMR and hydrogen/deuterium exchange detected by NMR show that the fold and a number of structural details are very similar for the prion domains of the two proteins. This structural similarity readily explains why cross-seeding occurs here in spite of the sequence divergence.

Keywords: prion; amyloid; fibrils; HET-s protein; FgHET-s protein

Introduction

Prions are infectious particles composed solely of protein.[1] In addition to the disease-causing mammalian prions, prions have also been identified in yeast and fungi. These prions represent interesting model systems to study the process of prion propagation.[2] The [Het-s] prion of the filamentous fungus *Podospora anserina* is involved in a non-self-recognition process termed heterokaryon incompatibility that operates when strains of unlike genotypes fuse and which leads to cell death of the fusion cell.[3] The *het-s* gene locus has two alternate incompatible alleles designated *het-s* and *het-S* that encode for the proteins HET-s and HET-S, respectively. Strains expressing HET-s in its soluble form are termed [Het-s*]; strains expressing the fibrillar prion form of HET-s are designated [Het-s]. It is the prion

*Corresponding author. E-mail address: beme@ethz.ch.
Present address: R. Sabaté, Departament de Bioquímica I Biologia Molecular and Institut de Biotecnologia i de Biomedicina, Universitat Autònoma de Barcelona, 08193 Bellaterra (Barcelona), Spain.

Abbreviations used: 3D, three-dimensional; INEPT, insensitive nuclei enhanced by polarization transfer; DARR, dipolar-assisted rotational resonance; MIRROR, mixed rotational and rotary resonance; TOBSY, total through-bond correlation spectroscopy; SPINAL, small phase incremental alternation; ThT, thioflavin T; DMSO, dimethyl sulfoxide; H/D, hydrogen/deuterium; CP, cross-polarization; MAS, magic-angle spinning; RF, relative fluorescence.

0022-2836/$ - see front matter

form [Het-s] that shows the heterokaryon incompatibility reaction with [Het-S].

HET-s represents an attractive model to study the sequence–structure relationship in amyloidal prions. Fibrils formed *in vitro* from the prion domain HET-s (218–289)[4] feature a highly ordered, triangular amyloid core of which an atomic resolution structure has been determined.[5] It can be described as a β-solenoid (see Ref. 6 for definition) where one molecule forms two windings. In addition to the rigid, highly ordered core region, HET-s(218–289) also contains a dynamically disordered flexible loop, comprising residues 250–259.[7,8] This fold of the isolated prion domain is maintained in the context of the full-length prion.[9]

In this article, we describe a distant homologue of the fungal prion HET-s found in the filamentous euascomycete *Fusarium graminearum*, which is a prominent wheat, barley, oat, and maize pathogen.[10] As HET-s, the homologue, which we denote by FgHET-s, comprises 289 amino acid residues but both proteins display a sequence identity of only about 50% for all residues and 38% for the prion domain (residues 218–289). While FgHET-s has not been tested for prion activity in its native host, we show below that recombinant FgHET-s(218–289) can form amyloid fibrils *in vitro*. These fibrils are able to efficiently cross-seed HET-s(218–289) fibril formation (and *vice versa*).

In the following, hydrogen/deuterium (H/D) exchange and solid-state NMR data from FgHET-s (218–289) are found to be remarkably similar to those of HET-s(218–289) fibrils, despite the rather low sequence identity. Based on these data, we propose a structural model based on HET-s, which shares important features, such as the hydrophobic core and lattices of water-exposed salt bridges. Our findings provide a structural basis for the observed efficient cross-seeding of the amyloid form.

Results

Sequences homologous to the HET-s prion domain exist in various *Fusarium* species

Searching the available fungal genomic databases at the National Center for Biotechnology Information and Broad Fungal Genome Initiative with the HET-s prion domain as query in Basic Local Alignment Search Tool Proteins searches, we identified homologous sequences in various *Fusarium* species, namely, *F. graminearum* (*Gibberella zeae*), *F. verticillioides* (*Gibberella moniliformis*), *F. oxysporum*, and *Nectria haematococca* (*Fusarium solani*). An alignment of the sequences of the C-terminal region of *Fusarium* proteins showing homology to HET-s(218–289) is given in Fig. 1. The closest homologue is found in *F. graminearum*. The predicted protein FG10600 was considered as the *F. graminearum* HET-s based on the reciprocal best hit method[12] and will be referred to as FgHET-s in the following. Overall HET-s and FgHET-s show 50% identity (55% in the globular domain and 38% in the region corresponding to the prion domain). The C-terminal region of FgHET-s [FgHET-s(218–289)] is the closest homologue to the HET-s prion domain identified in this search and was chosen for further characterization.

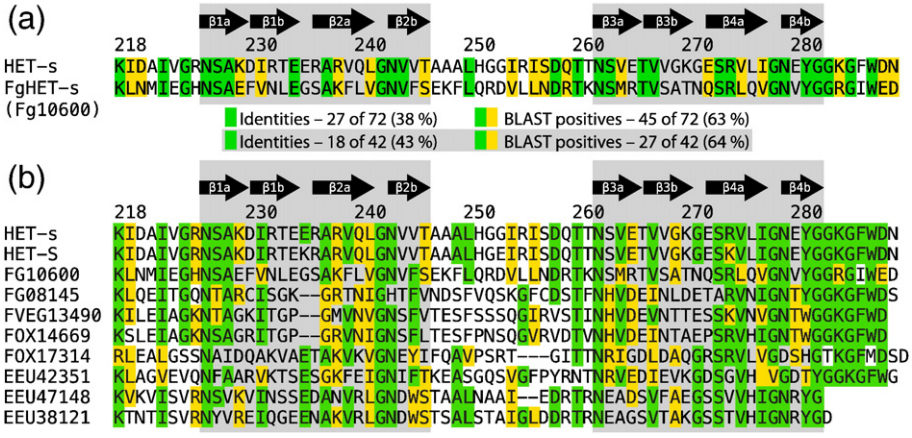

Fig. 1. Sequence alignments of the C-terminal region of HET-s and homologues from different *Fusarium* species. The primary structure of HET-s(218–289) is compared to (a) FgHET-s(218–289) only and to (b) known HET-s homologues. Residues highlighted in green or yellow are identical or have preserved physicochemical properties (BLAST positives), respectively.[11] The sequence designation of the Fusarium homologues corresponds to the GenBank accession numbers. FG10600 and FG08145 are from *F. graminearum*, FOX17314 and FOX14669 from *F. oxysporum*, FVE13490 from *F. verticillioides*, and EEU42351, EEU47148, and EEU38121 from *N. haematococca* (*Fusarium solani*). On top of the alignment, the secondary-structure elements described in the HET-s(218–289) β-solenoid structure in Ref. 5 are given.

Recombinant FgHET-s(218–289) forms amyloid fibrils *in vitro*

In order to analyze the properties of the FgHET-s prion domain, we expressed the region corresponding to the HET-s prion domain FgHET-s(218–289) as previously described for HET-s(218–289) with a C-terminal histidine$_6$ tag and purified it under denaturing conditions from inclusion bodies.[4] Similar to HET-s(218–289), FgHET-s(218–289) remained soluble at acidic pH (175 mM acetic acid, pH 2.5) but spontaneously aggregated into amyloid fibrils at pH 7 at 20 μM. Similar to HET-s(218–289) fibrils formed under the same buffer conditions, FgHET-s(218–289) formed bundles of laterally associated individual fibrils of about 5 nm width (Fig. 2a). In contrast to HET-s(218–289) fibrils, which were reported not to induce thioflavin T (ThT) fluorescence,[13] FgHET-s (218–289) fibrils do induce a robust ThT fluorescence (Fig. 2b).

The stability of FgHET-s(218–289) fibrils against denaturation by both GuHCl and urea was probed by measuring tryptophan fluorescence at different concentrations of the respective denaturant. We found that FgHET-s(218–289) fibrils were denatured at significantly lower concentrations of both urea and GuHCl than HET-s(218–289) fibrils (Fig. 2c), indicating that FgHET-s(218–289) fibrils are less stable than HET-s(218–289) fibrils.

In vitro FgHET-s(218–289) fibrils seed HET-s (218–289) fibril formation and *vice versa*

Preformed HET-s(218–289) fibrils are able to suppress the lag phase observed during *in vitro* fibril formation.[4,13] We set out to determine whether cross-seeding between FgHET-s(218–289) and HET-s(218–289) is possible *in vitro* and observed that preformed FgHET-s(218–289) fibrils are able to accelerate HET-s (218–289) fibril formation and that, *vice versa*, HET-s

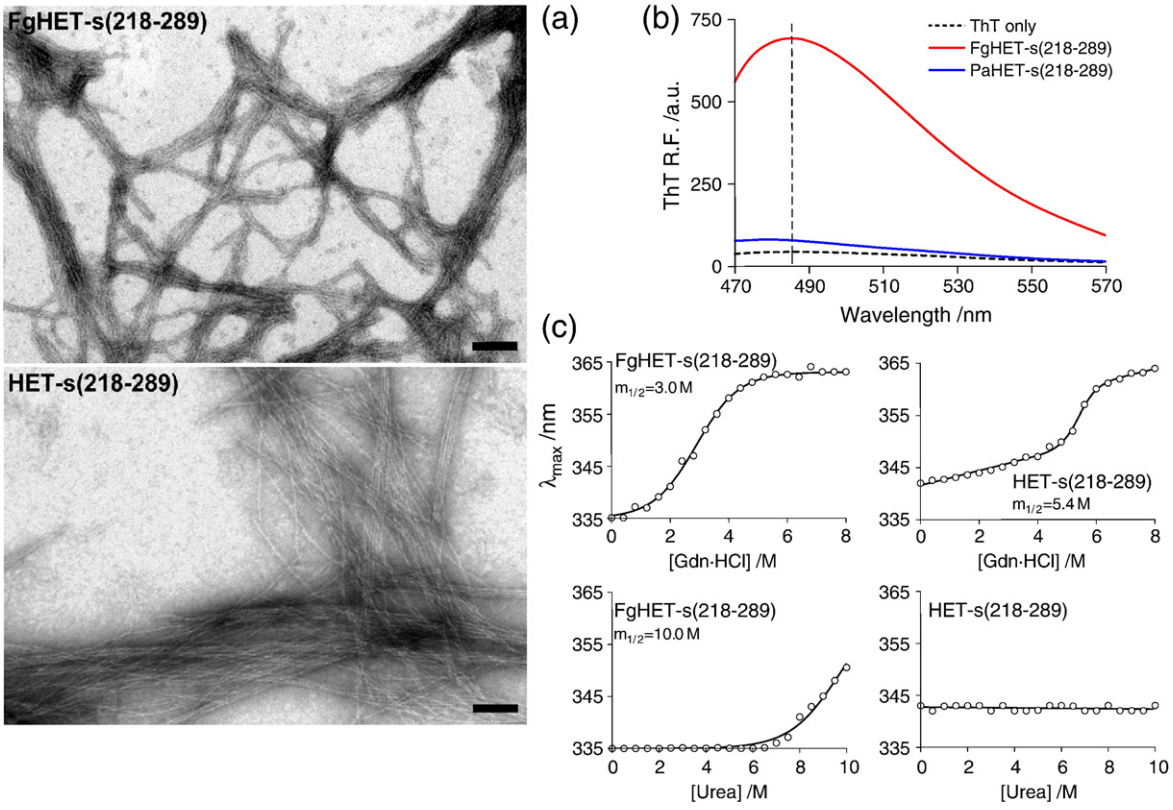

Fig. 2. FgHET-s(218–289) forms amyloid fibrils. (a) Electron micrograph of FgHET-s(218–289) and HET-s(218–289) fibrils (scale bars represent 25 nm). (b) ThT-induced fluorescence of FgHET-s(218–289) fibrils. Note that in contrast to FgHET-s(218–289) fibrils, HET-s(218–289) fibrils do not induce ThT fluorescence. The excitation wavelength was 450 nm and emission was recorded from 470 to 570 nm. ThT and protein concentrations of 25 and 10 μM, respectively, were used. The measurement was performed at both pH 4 and pH 7 and yielded basically identical results (see Supplementary Fig. S5). (c) GuHCl (top panels) and urea (bottom panels) induced chemical denaturation of FgHET-s(218–289) and HET-s(218–289) fibrils measured by shift in the maximum emission wavelength of the W287 residue at pH 7. Note that FgHET-s(218–289) are more sensitive than HET-s(218–289) fibrils to both chemical denaturants. As previously reported, no denaturation of HET-s(218–289) fibrils was detected in the presence of urea in these buffer conditions. For the actual UV absorption spectra, see Supplementary Figs. S6 and S7.

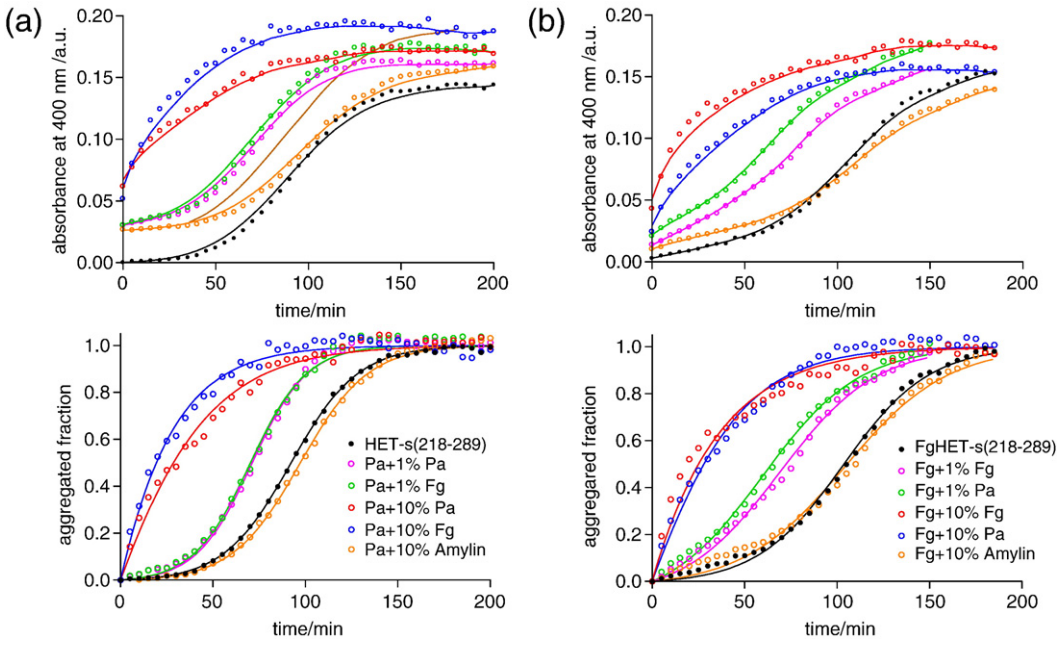

Fig. 3. *In vitro* cross-seeding between FgHET-s(218–289) and HET-s(218–289) fibrils. (a) Aggregation of HET-s(218–289) and (b) aggregation of FgHET-s(218–289) under the influence of different seeds (see legend to the figure). In the top panels, the time courses of the absorbance at 400 nm (raw data) during the fibrillization process are given. The two bottom panels show the normalized data. Note that all FgHET-s(218–289) fibril formation experiments were performed at pH 4.5 to increase the lag phase in spontaneous FgHET-s(218–289) fibril formation.

(218–289) fibrils accelerate FgHET-s(218–289) fibril formation (Fig. 3). Amyloid fibrils from the unrelated heterologous polypeptide amylin were used as a control and did not show a detectable effect on neither the HET-s(218–289) nor the FgHET-s(218–289) fibril formation rate. Also, seeding with fibrils of full-length Ure2p and Sup35 did not accelerate Het-s (218–289) or FgHET-s(218–289) fibril formation (data not shown). We conclude from these observations that *in vitro* cross-seeding between FgHET-s(218–289) and HET-s(218–289) readily occurs.

Quenched H/D exchange indicates the location of β-sheets in FgHET-s(218–289) fibrils

In order to determine whether the observed cross-seeding between HET-s(218–289) and FgHET-s(218–289) *in vitro* is related to a similarity in the three-dimensional (3D) structures of the two fibrils, we performed quenched H/D-exchange experiments detected by NMR on FgHET-s(218–289) fibrils. H/D exchange is a sensitive tool for the sequence-specific identification of secondary-structure elements, as backbone amide protons involved in H-bonds are protected from exchange with the solvent and particularly slow exchange is observed for β-sheets. Dimethyl sulfoxide (DMSO) can be used to solubilize amyloid fibrils into monomers, while preserving the protonation state that was present in the fibrils. This makes the H/D-exchange experiment amenable to a solution NMR analysis by recording fast heteronuclear multiple quantum coherence spectra of the ^{15}N-labeled protein. This technique has been successfully employed for the structural analysis of amyloid fibrils formed by HET-s(218–289) as well as a number of other amyloidogenic proteins.[14–18] Hydrogen exchange in D_2O buffer was followed over 12 weeks. After 4 weeks, the intensities of about 40% of the resonances were significantly reduced in the spectrum (Supplementary Fig. S1). This demonstrates that the corresponding amide protons had undergone exchange with solvent deuterons and were therefore no longer detectable in the NMR experiment. The approximately mono-exponential decay observed for all residues displaying significant hydrogen exchange during the analyzed time interval suggests a well-defined and homogenous structure of the fibrils.

The resulting exchange-rate constants are shown in Fig. 4c. The backbone amides of the five N-terminal residues, the seven C-terminal residues, and residues 246–258 exchanged quickly ($\geq 1.5\ h^{-1}$); that is, they are only weakly protected or not protected at all against the solvent. These residues seem to be not involved in any regular secondary-structure elements. We identified four segments displaying very slow exchange rates in the range of $10^{-5}\ h^{-1}$ to $10^{-2}\ h^{-1}$ in good agreement with the exchange-rate constants determined for the β-sheet regions of HET-s(218–289).[14] The four segments with protected amide hydrogen atoms comprise residues 223–234, 237–245, 259–270, and 273–282, which are thus considered to be involved in

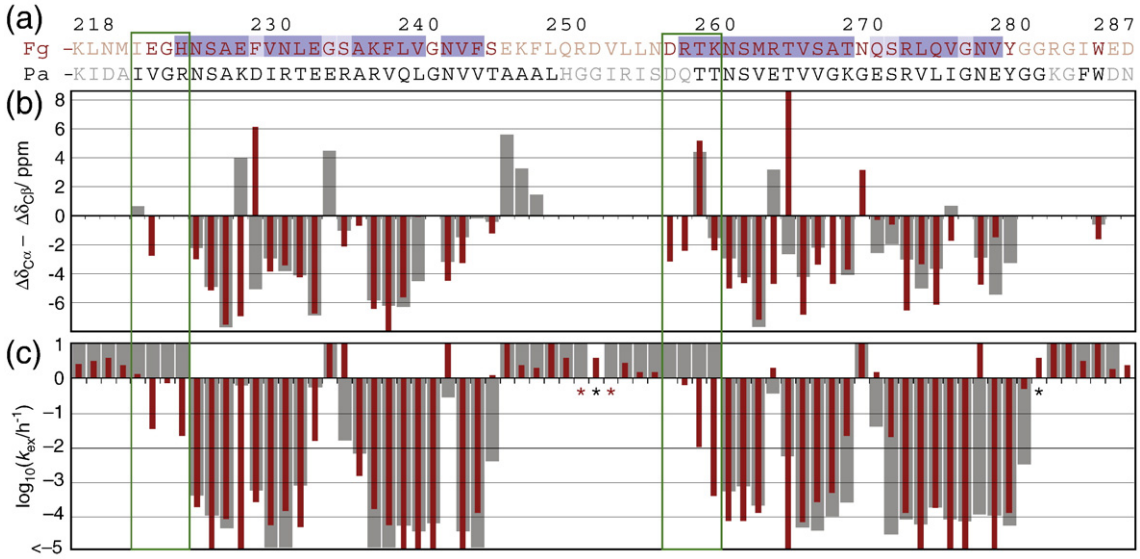

Fig. 4. H/D-exchange data and secondary-structure prediction. (a) Sequences of HET-s(218–289) and FgHET-s(218–289) with TALOS secondary-structure prediction.[19] Residues in dark and light blue show typical β-sheet backbone angles in 9 to 10 and 6 to 8 out of 10 predictions, respectively. (b) Difference of C^{α} and C^{β} secondary chemical shifts for residues with both C^{α} and C^{β} resonances assigned. Negative and positive values are typical for β-sheet and α-helical conformations, respectively.[20] (c) Red and gray bars give the H/D exchange rates for FgHET-s(218–289) and HET-s(218–289), respectively. For residues marked with a red or black asterisk, no H/D exchange data are available for FgHET-s(218–289) or HET-s(218–289), respectively.

hydrogen bonds. In HET-s(218–289), the protected stretches were identified as β-sheets. Within these highly protected regions, residues 243, 265, and 279 show fast exchange. These observations are similar to what has been found in HET-s(218–289), where three of the arcs between the sheets were characterized by a single unprotected residue.[5,14]

Solid-state NMR chemical shifts of FgHET-s (218–289) fibrils reveal high structural similarity with HET-s

To characterize the rigid parts of the FgHET-s (218–289) fibrils, we recorded solid-state NMR experiments employing an initial adiabatic-passage cross-polarization (CP) step[21,22] (from protons to either ^{13}C or ^{15}N) under magic-angle spinning (MAS). The CP transfer is mediated via the dipolar coupling between the involved nuclei and therefore most effective for rigid parts of the sample, while motion averages out this interaction and therefore quenches the transfer. For example, for HET-s(218–289), this kind of spectrum is almost exclusively sensitive for the core region of the amyloid fibrils, that is, residues 226–249 and 260–282. A CP-MAS solid-state NMR spectrum of U-[^{13}C,^{15}N] FgHET-s (218–289) amyloid fibrils, a ^{13}C–^{13}C correlation experiment with a 100-ms dipolar-assisted rotational resonance (DARR)[23,24] mixing period, is shown in Fig. 5a (the carbonyl region is shown in Supplementary Fig. S2). The spectral resolution is not as good as in HET-s(218–289) (Fig. 5b), with ^{13}C linewidths in the range of 100–200 Hz. For HET-s(218–289), the linewidth ranged between 40 and 100 Hz (comparison at $B_0 = 20.0$ T; only resolved peaks in the 100-ms DARR spectra of both samples were taken into account). The increase in linewidth, obtained under otherwise identical conditions, points to a somewhat increased structural heterogeneity of the FgHET-s (218–289) fibrils. Nevertheless, by employing 3D correlation spectroscopy to overcome spectral overlap, we could sequence-specifically assign the resonance frequencies of almost all visible peaks. Heteronuclear correlation spectra, namely, NCACX and NCOCX, were recorded with both two-dimensional (2D) and 3D acquisition schemes[25–29] and were most useful in the assignment process. An example of the assignment process is shown in Fig. 6. Additionally, a 100-ms DARR spectrum was used to verify backbone assignments and for the assignment of some side-chain atoms. Figure 7 shows the 2D N(CO)CX spectrum; both 2D ^{15}N–^{13}C correlation spectra with the assigned peaks labeled are shown in Supplementary Fig. S3. Essentially all peaks in the spectrum can be explained by the resonance assignment given in Supplementary Table S1. The details of the resonance assignment process are described in the Supplementary Information. Using all recorded spectra jointly, the resonance frequencies of 95% of the ^{15}N and ^{13}C backbone atoms (N, C′, C^{α}, and C^{β}) within the rigid stretches E223–S246, D258–Y281, and W287 could be assigned sequence specifically

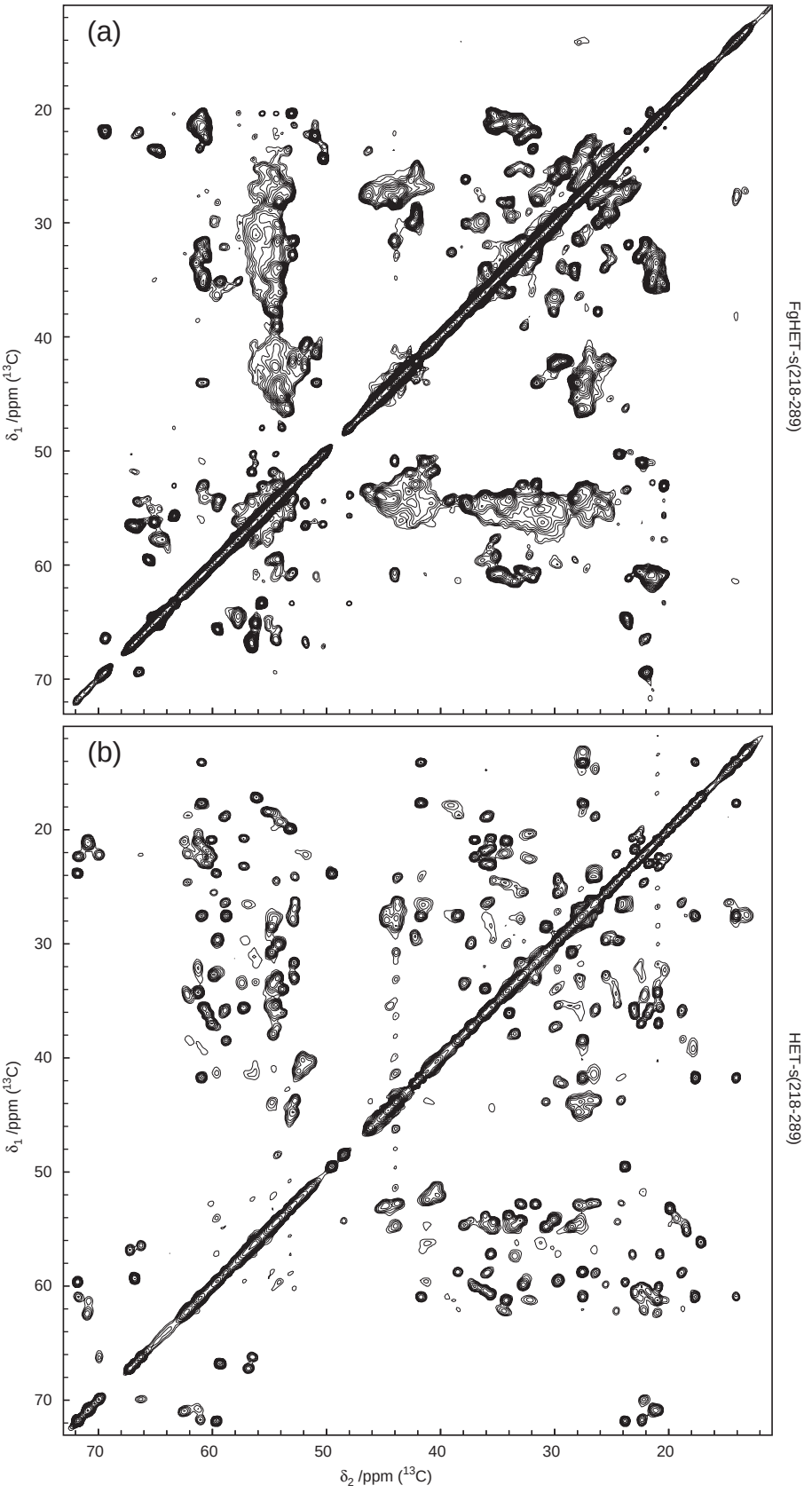

Fig. 5 (*legend on next page*)

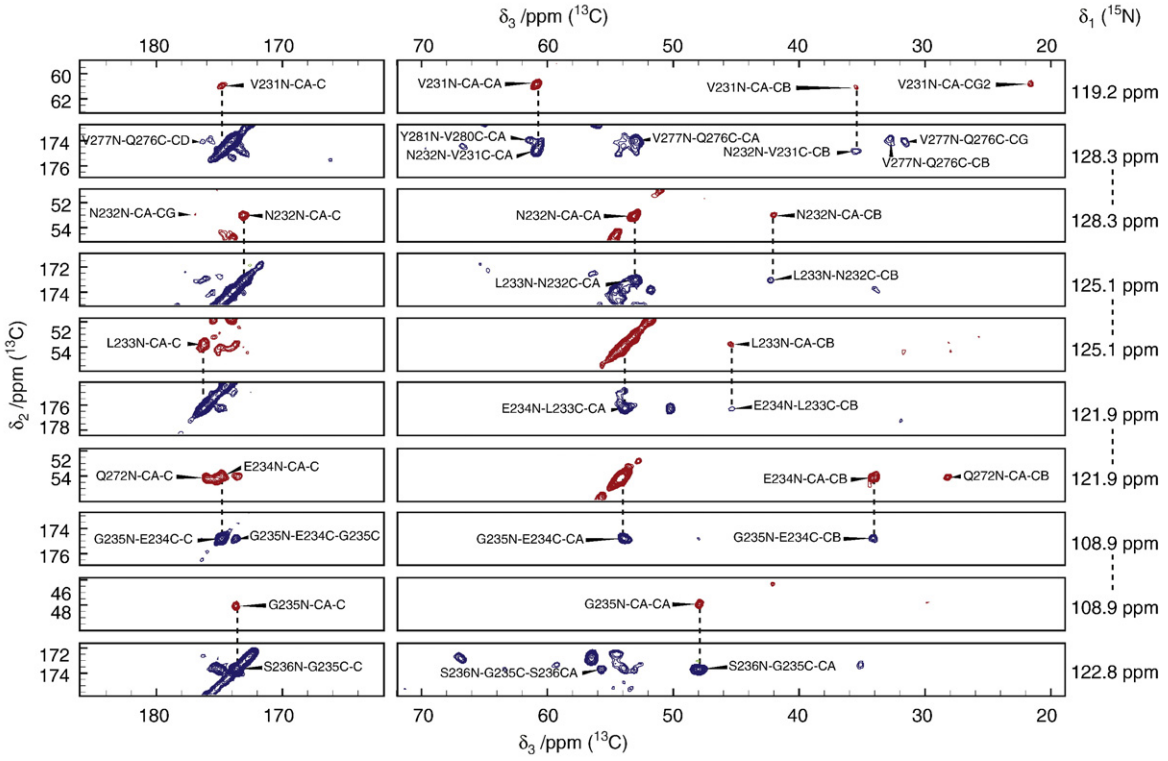

Fig. 6. Strip plots of the 3D NCOCX (blue contours) and 3D NCACX (red contours) spectra[29] used for the sequential assignment. The displayed sections illustrate the sequence-specific backbone-resonance assignment for the fragment V231-S236. The spectra were recorded at 850 MHz ^{1}H resonance frequency, 19 kHz MAS frequency, 4 ms N–C CP, 50 ms DARR/MIRROR C–C mixing, and 100 kHz SPINAL64 decoupling during t_1, t_2, and t_3.

(Fig. 4a; see Supplementary Table S1 for a complete list of assignments).

Due to the strong dependence of the chemical shifts on the polypeptide backbone conformation, these can be used to deduce information about the dihedral angles Φ and Ψ and to predict the secondary structure. To this aim, we applied the program TALOS[19] to the FgHET-s(218–289) chemical shifts (see Fig. 4a) and it yielded clear predictions for β-sheet conformation (9 or 10 out of 10 database matches) for residues H225-E229, V231-E234, A237-V241, N243-F245 and R259-T270, R274-V277, N279, and V280, and strong indications (6 to 8 out of 10 predictions) for β-sheet conformation for F230, G235, S236, Q272, S273, and G278. For residues G224, G242, and N271, the results were ambiguous. Note that TALOS cannot predict the conformation of E223, S246, D258, and Y281, as one neighboring residue of these is not assigned. No residue was predicted to have an α-helical conformation. Additionally, the secondary chemical shifts, meaning the deviation of the chemical shifts from their random-coil value (taken from Ref. 30) were evaluated, which are also indicative for secondary-structure elements. In particular, the difference of the C^{α} and C^{β} secondary chemical shift, which is positive if a residue is in an α-helical conformation and negative if it is in a β-sheet conformation,[20] has been calculated and analyzed. This value, $\Delta\delta_{C\alpha} - \Delta\delta_{C\beta}$ is negative for all residues except F230, T260, T266, and N271 (Fig. 4b, only residues with both C^{α} and C^{β} atoms assigned were taken into account). This confirms that FgHET-s(218–289) amyloid fibrils contain almost exclusively β-sheets as secondary-structure elements. From the analysis of the chemical shifts and structure of HET-s (218–289),[5] it is known that a single residue with a positive value $\Delta\delta_{C\alpha} - \Delta\delta_{C\beta}$ (e.g., K229 and E265) most likely designates the position of a β-arc.

To test for highly dynamical residues, we performed NMR experiments employing an initial H–C

Fig. 5. Aliphatic regions of a PDSD spectrum of U-[^{13}C,^{15}N]-labeled samples of (a) FgHET-s(218–289) and (b) HET-s (218–289) with 100 ms DARR mixing.[23,24] For these short mixing times, short-range (intra-residue and sequential) correlations are dominant. Spectrum (a) was used together with the NCACX and NCOCX spectra (Figs. 6 and 7 and Supplementary Fig. S3) for sequence-specific assignments. Both spectra were recorded at 850 MHz ^{1}H resonance frequency, 19 kHz MAS frequency, and with 100 kHz SPINAL64 decoupling during t_1 and t_2. Both aliphatic and carbonyl regions of the DARR spectrum of FgHET-s(218–289) are given in Supplementary Fig. S2.

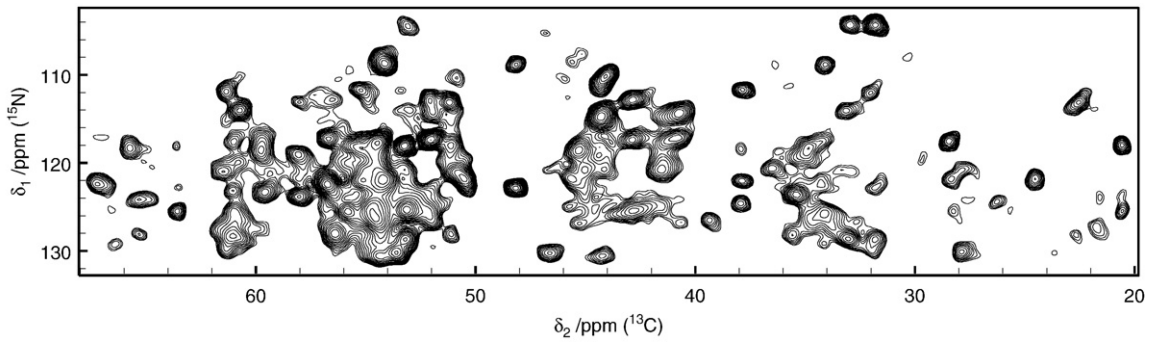

Fig. 7. Aliphatic region of the 2D N(CO)CX solid-state NMR spectrum.[25] The spectrum was recorded at 19 kHz MAS, B_0 = 20.0 T, and 50 ms DARR for the C–C mixing period. This spectrum and the N(CA)CX with peak labels are shown in the Supplementary Information.

insensitive nuclei enhanced by polarization transfer (INEPT) step[31,32] and detection on ^{13}C.[33,34] In contrast to the CP-type experiments described in the previous section, the INEPT is expected to transfer polarization exclusively for very dynamic moieties that possess sufficiently long transversal relaxation times (T_2). For HET-s(218–289), dynamic residues that most probably belong to either the N-terminus, a stretch comprising about residues 250–259, or the C-terminus could be detected.[7] The chemical shifts of the observed cross-peaks indicate a random-coil conformation for these parts of HET-s(218–289).

An H(C)C INEPT and an (H)CC INEPT experiment, both with additional homonuclear ^{13}C–^{13}C total through-bond correlation spectroscopy (TOBSY) transfer steps[35,36] after the initial INEPT, were recorded to facilitate the assignment of the resonances to amino acid spin systems (Fig. 8 and Supplementary Fig. S4). The INEPT spectra of FgHET-s(218–289) feature only a few detectable resonances that could be assigned to atoms in the side chains of the amino acids N or D, L, K, M, T, and V. Backbone resonances were only found for two H spin systems, most likely arising from the C-terminal H_6-tag. In comparison to HET-s(218–289),[7,34] significantly fewer signals are observed for FgHET-s(218–289), which indicates that less residues are flexible enough to show up in this type of experiments. The chemical shifts of the assigned resonances closely resemble the random-coil values.[30]

Cross-seeded fibrils adopt a similar structure as unseeded

The electron micrograph fluorescence of the seeded fibrils has very similar features as those of the unseeded fibrils for both HET-s(218–289) and FgHET-s(218–289) (Supplementary Fig. S8), and the FgHET-s(218–289) showed florescence with ThT, also if seeded with HET-s(218–289). The 100-ms DARR solid-state NMR spectrum of FgHET-s(218–289) fibrils was seeded by preformed HET-s(218–289). The spectrum (Supplementary Fig. S9) shows that the seeded fibrils exhibit the same chemical shifts as the unseeded ones and therefore also have the same structure. Nevertheless, some differences are found, in particular a broader lineshape for seeded sample, indicative of an increased disorder or polymorphic behavior (Supplementary Fig. S9). Detailed investigations of this phenomenon are presently under way.

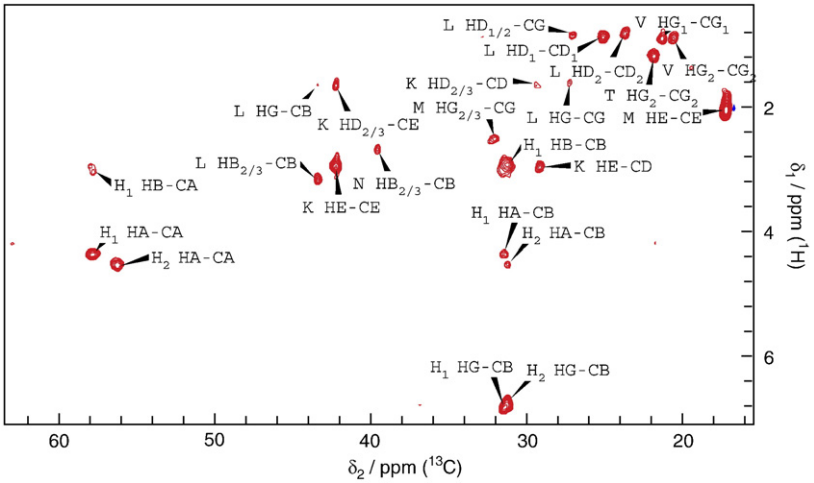

Fig. 8. Aliphatic region of the carbon-detected INEPT experiment with a homonuclear carbon TOBSY transfer performed on U-[^{13}C,^{15}N]-labeled FgHET-s(218–289) amyloid fibrils. This type of experiment is exclusively sensitive to highly dynamic parts of the protein.

Discussion and Conclusions

Structural comparison to HET-s(218–289)

The secondary chemical shifts as a function of the primary structure, as extracted from the solid-state NMR assignment of FgHET-s(218–289), closely resemble that of HET-s(218–289) (Fig. 4b). This implies that FgHET-s(218–289) contains β-sheet elements in almost the same positions as HET-s (218–289). The few residues with positive secondary chemical shift differences $\Delta\delta_{C\alpha} - \Delta\delta_{C\beta}$ (F230, T260, T266, and N271) most likely indicate the positions of β-arcs connecting sequentially adjacent β-strands [as also seen in HET-s(218–289)].[5,14] The lower protection from H/D exchange of these residues confirms this and indicates β-arcs at G235-S236, N243, R265, N271-Q272, and N279. The H/D-exchange data are more complete as no chemical shift analysis was performed for glycine residues that happen to be particularly abundant within (or just before) a β-arc. The fact that each of the β-arcs has a partner at ±36 residues [(F230, T266), (G235, N271), (N243, N279)] suggests that the two pseudo-repeats 223–245 and 259–281 form parallel β-sheets with one another as seen in HET-s(218–289).

The most obvious difference to HET-s(218–289) is the appearance of additional rigid residues in FgHET-s(218–289), namely, 223, 224, and 258–260, which could form a very short β-sheet and maybe a connecting β-arc (green boxes in Fig. 4). The reason for this might be found in the two oppositely charged residues E223 and R259, separated by exactly 36 residues[5] in the FgHET-s(218–289) sequence and therefore partners in a hypothetical additional N-terminal β-sheet. The side chains of these two residues may form a salt bridge and thereby stabilize the β-sheet. For HET-s(218–289), no such interaction is conceivable as valine and glutamine are the respective residues at positions 223 and 259 and accordingly residues 222–225 and 258–262 are not in a β-sheet. This finding is supported by the fact that H/D exchange is very fast here.[14]

In HET-s(218–289), residues 247 to 261 are only weakly protected from H/D exchange and only the beginning and end of this stretch are visible in CP-type solid-state NMR experiments, indicating a high degree of dynamics for residues in the center of the loop.[7] Indeed, these residues in HET-s(218–289) are observable in INEPT experiments. For FgHET-s(218–289), on the other hand, no residues flexible enough to show backbone atoms in INEPT spectra were detected in the loop pointing towards a shorter, less flexible loop. All residues detected in the INEPT experiment show nearly the average chemical shift values (according to the Biological Magnetic Resonance Data Bank;[37] except for one His, which may be located in the C-terminal His_6-tag), which indicates that these residues are indeed flexible and not part of a highly dynamic but folded domain.

A remarkable difference between FgHET-s(218–289) and HET-s(218–289) occurs in the core region that otherwise seems to have a highly conserved structure between the proteins. The first β-arc is positioned at residues K229-D230 and E265-T266 for HET-s(218–289).[5] In FgHET-s(218–289), the position where the secondary chemical shifts deviate significantly from the values expected for a β-sheet is shifted by one residue, while the H/D exchange data show fast exchange at the same positions (see discussion below). This behavior could be explained by the fact that multiple types of two-residue β-arcs exist. Whereas a so-called ab arc[38] occurs at this position in HET-s(218–289), a bl arc, the most abundant form, could be present in FgHET-s(218–289). This arrangement would show basically identical side-chain arrangement (inside *versus* outside) but different backbone angles for E229 and F230 (R265 and T266), that is, a change in the consecutive dihedral angles Ψ_{229} and Φ_{230} (Ψ_{265} and Φ_{266}) of about 180°. This arrangement could explain the observed differences in the secondary chemical shifts.[39]

The finding that E229, positioned at this β-arc, is highly protected from H/D exchange, while the expected partner R265 has a high H/D-exchange rate can only be explained by differences in the H-bonding pattern occurring in the β-arcs at these positions. A similarly high protection of a residue within a β-arc has been observed for HET-s(218–289), where N243, connecting β2a and β2b, displays relatively fast hydrogen exchange, while the corresponding residue N279 connecting β4a and β4b is fully protected. A more detailed explanation has to await the full structure determination.

Another notable difference between the two fibrils is observed at the end of the first pseudo-repeat, around residues 246–249. In HET-s(218–289), three alanine residues occupy positions 247–249 that, despite being unprotected from H/D exchange, are visible in CP-type spectra and exhibit chemical shifts typical of α-helices.[14] In FgHET-s(218–289), already the primary structure of this part, as well as of the whole flexible loop, does not bear any resemblance to HET-s(218–289). Also, there is no evidence in the CP spectra of the corresponding residues E247, K248, and F249, and therefore, these are likely to be dynamically disordered.

In addition to the two pseudo-repeat regions, there is only a single additional amino acid residue assigned in the CP-type spectra of FgHET-s(218–289). W287 is a conserved residue in most HET-s homologues (Fig. 1b) and is also present in HET-s (218–289) itself. The tryptophan side chain has been found to make contact with residues in β2a and β4a, one of the β-sheets confining the hydrophobic core region in HET-s(218–289) (H. Van Melckebeke *et al.*,

unpublished results) and this residue is necessary for the prion infectivity and *in vivo* aggregation of HET-s (S. Cescau and S.J.S., unpublished results). This residue, except for a few resonances of the side chain of the neighboring F286 in HET-s, is the only observable moiety of the C-terminus in CP-type NMR spectra of both FgHET-s(218–289) and HET-s (218–289). Therefore, it has to be at least partially immobilized in both protein fibrils underlining its importance for fibril formation.

Assuming the same fold for the core region 226–244/262–280 of FgHET-s(218–289) and HET-s(218–289) as depicted in Fig. 9, the resulting organization of hydrophobic and hydrophilic side chains in FgHET-s(218–289) is quite similar to HET-s(218–289). In detail, the hydrophobic core of FgHET-s (218–289) has to accommodate only 1 polar but 11 non-polar (2 polar and 10 non-polar in HET-s) amino acid side chains, whereas those pointing outside are, except for one (F230), either polar or charged, making the model rather appealing.

Another stabilizing feature observed for HET-s (218–289) fold is the possible formation of three inter-β-strand salt bridges between the oppositely charged side chains of K229-E265, E234-K270, and R236-E272 that may form both intra- and intermolecularly.[8] Only one of these is reproduced in the FgHET-s(218–289) homology model (Fig. 9), namely, between E229 and R265, with the charges inverted compared to HET-s(218–289). An additional pair of oppositely charged residues, E223-R259, may form a second salt bridge and might be the stabilizing element leading to the prolongation of β-sheet 1a/3a or the addition of a short β-sheet in FgHET-s(218–289). Whether the reduction of stability of the FgHET-s(218–289) fibrils (Fig. 2c) is indeed a direct consequence of the lower amount of possible salt bridges remains to be determined. The broader spectral lines in the solid-state NMR spectra of FgHET-s(218–289) could be attributed to a higher degree of conformational disorder, which might be related to a lower fibril stability or the smaller number of specific interactions that must be met by the structure to avoid significant energetic penalties.

The comparison of the structural models for HET-s(218–289) and FgHET-s(218–289) also allows to propose an explanation for the different behavior of the two proteins regarding the induced ThT fluorescence. It has been proposed that ThT binds amyloids in the "channels" running along the fibril

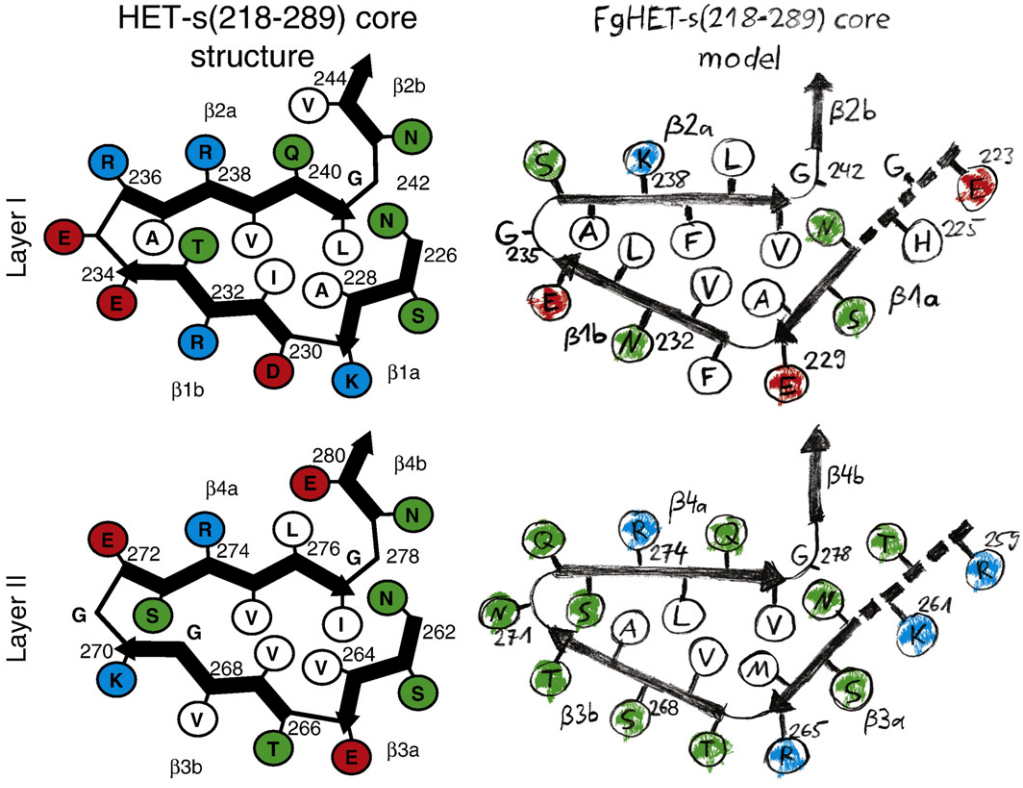

Fig. 9. Schematic representation of the two layers of the structure of the well-ordered hydrophobic core of HET-s(218–289) amyloid fibrils[5] (left half). This fold would explain all currently available data and is compatible with the primary structure of FgHET-s(218–289) as well (right). Circles representing positively or negatively charged residues are colored blue or red, respectively; polar but uncharged residues are green and non-polar residues are white.

axis delimited by the side chains of the i and $i+2$ residues of each β-strand.[40] ThT is positively charged, and thus, positively charged residues hinder ThT binding. All "channels" formed in HET-s(218–289) are lined by at least one positively charged residue, while, in contrast, in the FgHET-s (218–289) model, several of the accessible "channels" are free of basic residues. This observation might explain why, in spite of their overall structural similarity, FgHET-s(218–289) fibrils robustly induce ThT fluorescence while HET-s(218–289) fibrils fail to do so.

Evolutionary conservation of the β-solenoid fold

We have shown that FgHET-s(218–289) has the ability to form amyloids that are structurally highly similar to the HET-s(218–289) β-solenoid fold. The apparent structural similarity of the FgHET-s(218–289) and the HET-s(218–289) fibrils may seem surprising given the relatively low sequence identity of the two constructs (38%). A closer look however reveals that most of the conserved regions lie within the rigid and well-defined parts, the two pseudo-repeat regions 222–247 and 258–283, which have 43% sequence identity (green in Fig. 1a). Non-conserved residues with similar physicochemical properties (BLAST "positives", yellow in Fig. 1) are however scattered over the whole sequence. The sequence alignment shown in Fig. 1b reveals that the conservation of residues that play a key role in the β-solenoid fold of HET-s(218–289) extends to other identified *het-s* homologues in *Fusarium* species. For instance, the asparagine residues, which form two ladders along the fibrils axis in HET-s(218–289) (N226, N243 and N262, N279), are conserved in all homologues. The same is true for the G240 and G278 residues, allowing the formation of the β-arc leading into the fourth strand pointing away from the triangular hydrophobic core. Inward-facing hydrophobic residues in each β-strand of HET-s(218–289) (A228/V264, I231/V267, V239/V275, L241/I277) also show conservation in all *Fusarium* homologues. Finally, the C-terminal glycine-rich loop containing W287, which has been found to make contact with residues in β2a and β4a (H. Van Melckebeke *et al.*, unpublished results), is also conserved in many homologues (with the exception of two *Nectria* sequences). These observations strongly suggest that a selective pressure to maintain the ability to form this β-solenoid structure, including the C-terminal residues, is operating. The estimated divergence time between *P. anserina* and *F. graminearum* is roughly in the range of 400 MYrs. During this period, the sequences of HET-s and FgHET-s have highly diverged, but in a way that allows to conserve amino acid positions important for the formation of the β-solenoid fold.

Structural similarity explains amyloid cross-seeding between HET-s(218–289) and FgHET-s(218–289)

Amyloid cross-seeding between HET-s(218–289) and FgHET-s(218–289) occurs in spite of a considerable divergence of the primary sequence. Our structural analysis provides a simple explanation for this cross-seeding ability: the actual structural similarity between HET-s(218–289) and FgHET-s (218–289) fibrils. This result suggests that amyloid templating is possible at moderate levels of sequential identity if structural similarity is ensured. Some indications of an increase in structural disorder are found for the seeded fibrils, and this observation will be followed up.

Summary

We conclude that, on a structural level, FgHET-s (218–289) is closely related to HET-s(218–289). In particular, hydrogen exchange and NMR chemical shifts indicate that the triangular hydrophobic core is conserved and that the major elements that additionally stabilize the core of the fibrils in HET-s(218–289), namely, at least 21 hydrogen bonds per molecule and one of the three salt bridges in HET-s (218–289), are conserved. The similarity of the structural models could explain the observation that *in vitro* cross-seeding is possible, even though the HET-s(218–289) and FgHET-s(218–289) proteins only exhibit moderate levels of sequence identity. On a more general level, our study illustrates the fact that two amyloid proteins sharing 38% sequence identity can adopt highly similar structures. It is largely documented that homology levels in the range of 30% can lead to similar structures in soluble proteins.[41,42] Here, we present an example in which the same principle is applicable to amyloid structures despite the known tendency of amyloids to form different polymorphic forms and the fact that even point mutations have been shown to lead to completely different structures, for example, parallel and antiparallel β-sheets.[43]

Materials and Methods

Plasmids and strains

The *F. graminearum het-s* homologue has been cloned by PCR on genomic DNA of strain PH-1 (NRRL 31084) (genomic DNA prep was a generous gift of Jin-Ron Xu, Purdue University) using the following primers: 5′ TTCCAACAATAGCTAACCGC3′ and 5′ATTCAACACAGCCAACCGGC3′. The PCR fragment was cloned in the pGEM-T vector (Promega). The pET-24a-FgHET-s (218–289) plasmid was constructed by amplifying the

region encoding for the C-terminal part of the protein (residue 218 to 289) by PCR using primers 5′ATCATATGAAGTTGAACATGATCGAGG 3′ and 5′ATAAGCTTAATGGTGATGGTGATGGTGATCTTCCCAGATGCCTCTGCC3′. The PCR fragment was restricted by NdeI and HindIII and cloned into the pET-24a vector (Novagen).

Protein expression

For expression of HET-s(218–289)[44] and FgHET-(218–289), 2 l DYT medium was inoculated with an overnight culture of BL21(DE3) pLysS cells bearing the plasmids to be expressed at 37 °C. When an OD_{600} (optical density at 600 nm) of 0.6–0.8 was reached, the bacteria were induced with 1 mM IPTG. After 3 h at 37 °C, the cultures were centrifuged and the cell pellets were frozen at −20 °C.

Protein purification

HET-s(218–289) and FgHET-s(218–289) proteins expressed as a C-terminal histidine-tagged construct were purified under denaturing conditions [50 mM Tris/HCl (pH 8), 300 mM NaCl, and 6 M GuHCl buffer] by affinity chromatography on Talon histidine-tag resin (ClonTech). Buffer was exchanged by gel filtration on Sephadex G-25 column (Amersham) for 175 mM acetic acid (pH 2.5) and the proteins were conserved at 4 °C.

Amylin peptide (QRLANFLVHSSNNFGAILSS) was obtained from EZ Biolab Inc. (Carmel, IN, USA). A 5-mM stock solution was prepared in 1,1,1,3,3,3-hexafluoro-2-propanol, which had been sonicated two times for 30 min and dried at 4 °C and then had been centrifuged at 15,000*g* for 15 min, and was finally filtrated by Millex-GV 0.22-μm filters in order to remove possible residual quantities of large aggregates. After drying, the solution was incubated at room temperature for 10 min. Stock solutions were divided into aliquots (20 μl per eppendorf) and 1,1,1,3,3,3-hexafluoro-2-propanol was removed by evaporation under a gentle stream of nitrogen, leaving a slight film; finally, the samples were stored at −80 °C. When required, the samples were resuspended in 50 μl of anhydrous DMSO and were sonicated for 10 min. Sonication was crucial to remove any traces of non-dissolved seeds that may resist solubilization. This preparation yielded amylin in monomeric form. Aliquots of amylines were added to 100 μM acetate buffer (pH 5.5) and 850 μM miliQ water, obtaining a final peptide concentration of 100 μM. Peptide aggregation from soluble monomer was monitored by measuring the transition from non-aggregated to aggregated state by relative ThT fluorescence at 480 nm when exciting at 445 nm. Amylin aggregation was carried out at 37 °C with a soluble monomer concentration of 15 μM.

ThT-binding determination

ThT binding with HET-s(218–289) or FgHET-s(218–289) was recorded using a Perkin-Elmer LS50 fluorescence spectrometer with an excitation wavelength of 450 nm and an emission range from 470 to 570 nm, and the emission at 480 nm was recorded. ThT and protein concentration of 25 and 10 μM, respectively, at pH 7 and 37 °C were used.

Electron microscopy

For electron microscopy, 400-mesh copper electron microscopy grids coated with a plastic film (Formvar) were used. A fraction of the protein suspension (at 1 mg/ml) was put onto the grid and sedimented during 10 to 30 min in a moist Petri dish to avoid rapid desiccation. Grids were then rinsed with 15–20 drops of freshly prepared 2% uranyl acetate in water and filtered with 0.22 μm Millipore, dried with filter paper, and observed with a Phillips TECNAI 12 Biowin electron microscope at 80 kV.

Aggregation assays

HET-s(218–289) and FgHET-s(218–289) aggregation from soluble monomers was monitored by measuring the transition from non-aggregated to aggregated state by UV/Vis absorbance at 280 nm (tryptophan–tyrosine peak plus scattering) and 400 nm (scattering of the sample). All experiments were carried out with 10 μM soluble monomer at 25 °C and agitation every 5 min (by brief vortex pulse) in order to homogenize the samples. HET-s(218–289) fibrillations were realized at pH 7 (in a 1:1 mixture of 175 mM acetic acid and 1 M Tris/HCl, pH 8).[13] Fusarium fibrillations were realized at pH 4 (in a 3:1 mixture of 175 mM acetic acid and 1 M Tris/HCl, pH 8) in order to avoid the spontaneous aggregation of FgHET-s(218–289). For seeding and cross-seeding aggregation assays, 1 μM (representing 10% of total protein concentration) of the respective other, preformed fibrils was added to an initially 10 μM protein solution. In addition, in order to confirm the seeding and cross-seeding capacity, we tested 0.1 μM (1% of total protein concentration) HET-s(218–289) and FgHET-s(218–289) fibrils.

Chemical denaturation curves

FgHET-s(218–289) and HET-s(218–289) stabilities in the presence of guanidine hydrochloride and urea were studied at pH 7. The fraction of denatured protein (f_D) was calculated from the fitted values using the equation $f_D = 1 - ((y_D - y)/(y_D - y_N))$, where y_D and y_N are the fluorescence maximum wavelengths or the relative fluorescence (RF) at a fixed wavelength of the denatured and native protein, respectively, and y is the fluorescence maximum wavelength or RF at a fixed wavelength of protein as a function of denaturant concentration. A nonlinear least-squares analysis was used to fit the denaturation curves to $y = \{(y_N + m_N \cdot [D]) + (y_D + m_D \cdot [D]) \cdot \exp[A \cdot ([D] - m_{1/2})/R \cdot T]\}/(1 + \exp[A \cdot ([D] - m_{1/2})/R \cdot T])$, where y represents the observed fluorescence maximum wavelength or RF at a fixed wavelength, y_N and y_D are the intercepts, m_N and m_D are the slopes of the pre- and post-transition baselines, [D] is the chemical denaturant concentration, $m_{1/2}$ is the denaturant concentration at the midpoint of the curve, and A is a constant generated by the fitting.[45–47]

H/D exchange

U-[^{13}C,^{15}N] and [^{15}N] FgHET-s(218–289) were recombinantly expressed in *Escherichia coli* and amyloid fibrils

were prepared as described for HET-s(218–289).[14] ^{15}N-labeled FgHET-s(218–289) fibrils were used for H/D exchange studies relating to the backbone amides.[18,48] The fibrils were pelleted at 20,800*g* for 4 min to start the exchange reaction and then washed in 50 mM Tris/HCl, pH 7.3, comprising 150 mM NaCl and D_2O as the solvent, pelleted again, and resuspended in the same buffer for incubation up to 12 weeks. Hydrogen exchange was quenched at suitable intervals by pelleting the fibrils at 20,800*g* for 4 min and freezing the pellet on liquid nitrogen. For NMR analysis, the fibrils were solubilized in perdeuterated DMSO (d_6-DMSO) containing 0.05% deuterated trifluoric acid (d_1-TFA). Afterwards, a series of 80 2D [^{15}N, ^{1}H] correlation spectra were recorded for 4 h (3 min per spectrum) on a Bruker AVANCE III 600 spectrometer equipped with a CryoProbe unit. The amount of residual D_2O in DMSO was about 4%. Residues displaying fast exchange in the fibrils as well as residues with high intrinsic exchange rates in DMSO result in absent peaks in the [^{15}N,^{1}H] correlation spectrum. To identify the latter, we measured a second series of 80 2D spectra after the addition of 4% H_2O. Using identical solvent conditions as for hydrogen-exchange NMR analysis, we carried out triple-resonance HNCACB[49] and HNH nuclear Overhauser enhancement spectroscopy[50] experiments on U-[^{13}C,^{15}N] FgHET-s(218–289) to achieve the sequence-specific resonance assignment of the backbone amide moieties. All residues except for R252 could be assigned. [^{15}N,^{1}H] correlation spectra (Supplementary Fig. S1) were used to quantify the residual protonation depending on incubation time by integrating the peak volumes. To determine the specific exchange rates, we fitted these data to a mono-exponential decay. The data were analyzed by using the programs PROSA[51] and CARA[52] and a specially written Visual Basic program.[15] The resonances of N243 and N279 overlapped strongly. Since both residues displayed fast exchange and are located at identical positions within the repeat units, an average exchange rate for both residues was calculated.

Solid-state NMR

U-[^{13}C,^{15}N] FgHET-s(218–289) was recombinantly expressed in *E. coli*, and amyloid fibrils were prepared as described for HET-s(218–289).[14] These were washed in pure water and centrifuged into a 3.2-mm NMR rotor at 200,000*g*.[53] All solid-state NMR experiments were carried out on a Bruker AVANCE II+ wide-bore spectrometer with 850 MHz proton frequency (B_0 = 20.0 T) equipped with a 3.2-mm triple-resonance MAS probe. The MAS frequency was stabilized at 19.00 kHz, the sample temperature was ~3 °C, and small phase incremental alternation (SPINAL)64 proton decoupling of ~100 kHz was applied for all spectra. 2D and 3D NCACX and 2D and 3D NCOCX spectra[25,29] and a 2D C–C homonuclear correlation spectrum with 100-ms DARR/mixed rotational and rotary resonance (MIRROR) mixing[23,24] (simply called DARR in the following text) were recorded. Each of the two 3D experiments was acquired within 4 days of measurement time, the 2D N(CA)CX and N(CO)CX within 3 days each, and the DARR spectrum in 14 h. The ^{13}C–^{13}C polarization transfer in between carbonyl and aliphatic carbons was found to be optimal for a ^{1}H RF field irradiation of about 15 kHz during the mixing period (neither exactly at the DARR nor the MIRROR condition). A length of 50 ms was chosen for these homonuclear transfer steps.

While the 2D spectra exhibit a higher signal-to-noise ratio, the resolution of peaks is superior in the 3D experiments. Most of the sequence-specific assignments were made using the NCOCX and NCACX 3D-correlation spectra while the ^{13}C–^{13}C DARR spectrum was primarily used for verification and side-chain assignments.

In order to detect highly flexible residues, experiments employing an initial INEPT[31,32] with detection on ^{13}C[33] were carried out at 17 kHz MAS, a sample temperature of ~20 °C, and SPINAL64 proton decoupling of ~50 kHz at a static magnetic field of 20.0 T. In order to accomplish the spin-system resonance assignment, we added a ^{13}C–^{13}C transfer step to the initial ^{1}H–^{13}C INEPT. This homonuclear transfer was realized by a 5-ms TOBSY mixing period employing the $P9_3^1$ sequence[36] with an RF field of 102 kHz on ^{13}C. Topspin 2.0 (Bruker Biospin) was used to process all spectra and Sparky 3.113 (T. D. Goddard and D. G. Kneller, University of California, San Francisco) for the sequence-specific resonance assignment.

Acknowledgements

This work has been supported by the Eidgenössische Technische Hochschule Zurich through the ETHIRA grant system, the Centre National de la Recherche Scientifique, and the Helmholtz-Gemeinschaft. R. Sabaté was supported by the TRANS-DEATH EC grant. The authors thank Dr. René Verel for technical help.

Supplementary Data

Supplementary data associated with this article can be found, in the online version, at doi:10.1016/j.jmb.2010.06.053

References

1. Prusiner, S. B., Scott, M. R., DeArmond, S. J. & Cohen, F. E. (1998). Prion protein biology. *Cell*, **93**, 337–348.
2. Wickner, R. B., Edskes, H. K., Shewmaker, F. & Nakayashiki, T. (2007). Prions of fungi: inherited structures and biological roles. *Nat. Rev. Microbiol.* **5**, 611–618.
3. Coustou, V., Deleu, C., Saupe, S. & Begueret, J. (1997). The protein product of the het-s heterokaryon incompatibility gene of the fungus *Podospora anserina* behaves as a prion analog. *Proc. Natl Acad. Sci. USA*, **94**, 9773–9778.
4. Balguerie, A., Dos Reis, S., Ritter, C., Chaignepain, S., Coulary-Salin, B., Forge, V. *et al.* (2003). Domain organization and structure–function relationship of the HET-s prion protein of *Podospora anserina*. *EMBO J.* **22**, 2071–2081.

5. Wasmer, C., Lange, A., Van Melckebeke, H., Siemer, A. B., Riek, R. & Meier, B. H. (2008). Amyloid fibrils of the HET-s(218–289) prion form a beta solenoid with a triangular hydrophobic core. *Science*, **319**, 1523–1526.
6. Kajava, A. V. & Steven, A. C. (2006). Beta-rolls, beta-helices, and other beta-solenoid proteins. *Adv. Protein Chem.* **73**, 55–96.
7. Siemer, A. B., Arnold, A. A., Ritter, C., Westfeld, T., Ernst, M., Riek, R. & Meier, B. H. (2006). Observation of highly flexible residues in amyloid fibrils of the HET-s prion. *J. Am. Chem. Soc.* **128**, 13224–13228.
8. Lange, A., Gattin, Z., Van Melckebeke, H., Wasmer, C., Soragni, A., van Gunsteren, W. F. & Meier, B. H. (2009). A combined solid-state NMR and MD characterization of the stability and dynamics of the HET-s (218–289) prion in its amyloid conformation. *ChemBioChem*, **10**, 1657–1665.
9. Wasmer, C., Schütz, A., Loquet, A., Buhtz, C., Greenwald, J., Riek, R. *et al.* (2009). The molecular organization of the fungal prion HET-s in its amyloid form. *J. Mol. Biol.* **394**, 119–127.
10. Parry, D., Jenkinson, P. & McLeod, L. (1995). Fusarium ear blight (scab) in small grain cereals—a review. *Plant Pathol.* **44**, 207–238.
11. Altschul, S. F., Madden, T. L., Schäffer, A. A., Zhang, J., Zhang, Z., Miller, W. & Lipman, D. J. (1997). Gapped BLAST and PSI-BLAST: a new generation of protein database search programs. *Nucleic Acids Res.* **25**, 3389–3402.
12. Moreno-Hagelsieb, G. & Latimer, K. (2008). Choosing BLAST options for better detection of orthologs as reciprocal best hits. *Bioinformatics*, **24**, 319–324.
13. Sabate, R., Baxa, U., Benkemoun, L., Sanchez de Groot, N., Coulary-Salin, B., Maddelein, M. *et al.* (2007). Prion and non-prion amyloids of the HET-s prion forming domain. *J. Mol. Biol.* **370**, 768–783.
14. Ritter, C., Maddelein, M. L., Siemer, A. B., Luhrs, T., Ernst, M., Meier, B. H. *et al.* (2005). Correlation of structural elements and infectivity of the HET-s prion. *Nature*, **435**, 844–848.
15. Luhrs, T., Ritter, C., Adrian, M., Riek-Loher, D., Bohrmann, B., Dobeli, H. *et al.* (2005). 3D structure of Alzheimer's amyloid-beta(1–42) fibrils. *Proc. Natl Acad. Sci. USA*, **102**, 17342–17347.
16. Vilar, M., Chou, H. T., Luhrs, T., Maji, S. K., Riek-Loher, D., Verel, R. *et al.* (2008). The fold of alpha-synuclein fibrils. *Proc. Natl Acad. Sci. USA*, **105**, 8637–8642.
17. Toyama, B. H., Kelly, M. J. S., Gross, J. D. & Weissman, J. S. (2007). The structural basis of yeast prion strain variants. *Nature*, **449**, 233–237.
18. Hoshino, M., Katou, H., Hagihara, Y., Hasegawa, K., Naiki, H. & Goto, Y. (2002). Mapping the core of the beta(2)-microglobulin amyloid fibril by H/D exchange. *Nat. Struct. Biol.* **9**, 332–336.
19. Cornilescu, G., Delaglio, F. & Bax, A. (1999). Protein backbone angle restraints from searching a database for chemical shift and sequence homology. *J. Biomol. NMR*, **13**, 289–302.
20. Spera, S. & Bax, A. (1991). Empirical correlation between protein backbone conformation and C. alpha. and C.beta. ^{13}C nuclear magnetic resonance chemical shifts. *J. Am. Chem. Soc.* **113**, 5490–5492.
21. Pines, A., Gibby, M. & Waugh, J. (1973). Proton-enhanced NMR of dilute spins in solids. *J. Chem. Phys.* **59**, 569–590.
22. Hediger, S., Meier, B. H. & Ernst, R. R. (1995). Adiabatic passage Hartmann–Hahn cross polarization in NMR under magic angle sample spinning. *Chem. Phys. Lett.* **240**, 449–456.
23. Takegoshi, K., Nakamura, S. & Terao, T. (2001). C-13–H-1 dipolar-assisted rotational resonance in magic-angle spinning NMR. *Chem. Phys. Lett.* **344**, 631–637.
24. Scholz, I., Huber, M., Manolikas, T., Meier, B. H. & Ernst, M. (2008). MIRROR recoupling and its application to spin diffusion under fast magic-angle spinning. *Chem. Phys. Lett.* **460**, 278–283.
25. Detken, A., Hardy, E. H., Ernst, M., Kainosho, M., Kawakami, T., Aimoto, S. & Meier, B. H. (2001). Methods for sequential resonance assignment in solid, uniformly ^{13}C, ^{15}N labelled peptides: quantification and application to antamanide. *J. Biomol. NMR*, **20**, 203–221.
26. Straus, S. K., Bremi, T. & Ernst, R. R. (1998). Experiments and strategies for the assignment of fully ^{13}C/^{15}N-labelled polypeptides by solid state NMR. *J. Biomol. NMR*, **12**, 39–50.
27. Rienstra, C., Hohwy, M., Hong, M. & Griffin, R. (2000). 2D and 3D N-15–C-13–C-13 NMR chemical shift correlation spectroscopy of solids: assignment of MAS spectra of peptides. *J. Am. Chem. Soc.* **122**, 10979–10990.
28. Hong, M. (1999). Resonance assignment of ^{13}C/^{15}N labeled solid proteins by two- and three-dimensional magic-angle-spinning NMR. *J. Biomol. NMR*, **15**, 1–14.
29. Siemer, A. B., Ritter, C., Steinmetz, M. O., Ernst, M., Riek, R. & Meier, B. H. (2006). ^{13}C, ^{15}N resonance assignment of parts of the HET-s prion protein in its amyloid form. *J. Biomol. NMR*, **34**, 75–87.
30. Wishart, D. S., Bigam, C. G., Holm, A., Hodges, R. S. & Sykes, B. D. (1995). ^{1}H, ^{13}C and ^{15}N random coil NMR chemical shifts of the common amino acids. I. Investigations of nearest-neighbor effects. *J. Biomol. NMR*, **5**, 67–81.
31. Morris, G. A. & Freeman, R. (1979). Enhancement of nuclear magnetic resonance signals by polarization transfer. *J. Am. Chem. Soc.* **101**, 760–762.
32. Burum, D. P. & Ernst, R. R. (1980). Net polarization transfer via a J-ordered state for signal enhancement of low-sensitivity nuclei. *J. Magn. Reson.* **39**, 163–168.
33. Andronesi, O. C., Becker, S., Seidel, K., Heise, H., Young, H. S. & Baldus, M. (2005). Determination of membrane protein structure and dynamics by magic-angle-spinning solid-state NMR spectroscopy. *J. Am. Chem. Soc.* **127**, 12965–12974.
34. Lange, A. & Meier, B. H. (2008). Fungal prion proteins studied by solid-state NMR. *C. R. Chim.* **11**, 332–339.
35. Baldus, M., Iuliucci, R. & Meier, B. H. (1997). Probing through-bond connectivities and through-space distances in solids by magic-angle-spinning nuclear magnetic resonance. *J. Am. Chem. Soc.* **119**, 1121–1124.
36. Hardy, E. H., Verel, R. & Meier, B. H. (2001). Fast MAS total through-bond correlation spectroscopy. *J. Magn. Reson.* **148**, 459–464.
37. Ulrich, E. L., Akutsu, H., Doreleijers, J. F., Harano, Y., Ioannidis, Y. E., Lin, J. *et al.* (2008). BioMagResBank. *Nucleic Acids Res.* **36**, D402–D408.

38. Hennetin, J., Jullian, B., Steven, A. C. & Kajava, A. V. (2006). Standard conformations of beta-arches in beta-solenoid proteins. *J. Mol. Biol.* **358**, 1094–1105.
39. Wishart, D. S. & Nip, A. M. (1998). Protein chemical shift analysis: a practical guide. *Biochem. Cell Biol.* **76**, 153–163.
40. Krebs, M. R. H., Bromley, E. H. C. & Donald, A. M. (2005). The binding of thioflavin-T to amyloid fibrils: localisation and implications. *J. Struct. Biol.* **149**, 30–37.
41. Chothia, C. & Lesk, A. M. (1986). The relation between the divergence of sequence and structure in proteins. *EMBO J.* **5**, 823–826.
42. Ginalski, K. (2006). Comparative modeling for protein structure prediction. *Curr. Opin. Struct. Biol.* **16**, 172–177.
43. Tycko, R., Sciarretta, K., Orgel, J. & Meredith, S. (2009). Evidence for novel β-sheet structures in Iowa mutant β-amyloid fibrils. *Biochemistry*, **48**, 6072–6084.
44. Dos Reis, S., Coulary-Salin, B., Forge, V., Lascu, I., Begueret, J. & Saupe, S. J. (2002). The HET-s prion protein of the filamentous fungus *Podospora anserina* aggregates in vitro into amyloid-like fibrils. *J. Biol. Chem.* **277**, 5703–5706.
45. Santoro, M. & Bolen, D. (1988). Unfolding free energy changes determined by the linear extrapolation method. 1. Unfolding of phenylmethanesulfonyl α-chymotrypsin using different denaturants. *Biochemistry*, **27**, 8063–8068.
46. Pace, C., Hebert, E., Shaw, K., Schell, D., Both, V., Krajcikova, D. *et al.* (1998). Conformational stability and thermodynamics of folding of ribonucleases Sa, Sa2 and Sa3. *J. Mol. Biol.* **279**, 271–286.
47. Koditz, J., Ulbrich-Hofmann, R. & Arnold, U. (2004). Probing the unfolding region of ribonuclease A by site-directed mutagenesis. *Eur. J. Biochem.* **271**, 4147–4156.
48. Li, R. & Woodward, C. (1999). The hydrogen exchange core and protein folding. *Protein Sci.* **8**, 1571–1590.
49. Wittekind, M. & Mueller, L. (1993). HNCACB, a high-sensitivity 3D NMR experiment to correlate amide-proton and nitrogen resonances with the alpha- and beta-carbon resonances in proteins. *J. Magn. Reson. Ser. B*, **101**, 201–205.
50. Diercks, T., Coles, M. & Kessler, H. (1999). An efficient strategy for assignment of cross-peaks in 3D heteronuclear NOESY experiments. *J. Biomol. NMR*, **15**, 177–180.
51. Guntert, P., Dotsch, V., Wider, G. & Wuthrich, K. (1992). Processing of multi-dimensional NMR data with the new software PROSA. *J. Biomol. NMR*, **2**, 619–629.
52. Keller, R. (2004). *The Computer Aided Resonance Assignment Tutorial.* CANTINA Verlag, Goldau, Switzerland.
53. Böckmann, A., Gardiennet, C., Verel, R., Hunkeler, A., Loquet, A., Pintacuda, G. *et al.* (2009). Characterization of different water pools in solid-state NMR protein samples. *J. Biomol. NMR*, **45**, 319–327.